DYNAMIC MODEL AND DRIVE OF MULTIPHASE YASA ELECTRIC MACHINE FOR ELECTRIC TRACTION

Ederson dos Reis[1], Rodrigo Parizotto[1], Lucas Rossato Rocha[2], Evandro Claiton Goltz[2], Rodrigo Padilha Vieira[2], Paulo Roberto Eckert[1]

[1]Universidade Federal do Rio Grande do Sul, Porto Alegre – RS, Brazil

[2]Universidade Federal de Santa Maria, Santa Maria – RS, Brazil

e-mail: edreis1510@gmail.com, roparizotto@gmail.com, lucas_rrocha@hotmail.com, evandro@inf.ufsm.br, rodrigovie@gmail.com, paulo.eckert@ufrgs.br

Abstract – **This work addresses the dynamic modeling and the drive of a multiphase YASA-type electric machine for use within electric traction. The main technical aspects of the machine, which can be fed with three or five phases depending on the electrical connection of its windings, are presented. The dynamic model of the machine for the two different electrical connections (three or five phases) is given in the synchronous reference frame and the parameters of the lumped model are obtained through experimental tests. In order to consider the vehicular application, standard driving cycles are used to serve as a reference for the speed whereas vehicular dynamics are considered to define the load torque to be developed by the machine. Afterward, field orientation control (FOC) is implemented for the machine to operate with three or five phases and simulations were carried out to show that the dynamic behavior is similar in both cases. Experimental tests validated the model and the FOC for the machine with both electrical connections. In addition, the reference curves of the driving cycle were satisfactorily followed, indicating the possibility of using the multiphase YASA machine with the control developed in vehicular traction applications.**

Keywords – **Driving cycles, Electric traction, Field Oriented Control, Multiphase machine, YASA machine.**

I. INTRODUCTION

A subject that has been causing great concern in the scientific community in the last decades is the environmental issues caused due to several factors such as CO2 and greenhouse gas emissions, shortage of fossil fuels, and the increase in pollution in large cities. In this context, the transport sector is responsible for up to 75 % of greenhouse gas emissions. Therefore, vehicle electrification is essential for reducing carbon emissions and consequently improving environmental conditions [1].

Electric vehicles bring benefits that include zero direct emissions and better efficiency compared to combustion vehicles. Several countries have announced targets for 100 % zero-emission vehicles and the elimination of fuel-powered vehicles. Tax incentives on purchases and complementary measures such as toll discounts are important to attract consumers and companies to choose the electric option [2].

The expansion in the production of electric vehicles encouraged researchers to investigate and develop electric powertrains with optimized features. Additionally, specific requirements for electrification in different areas such as automotive, naval, and aerospace [3] have also boosted related studies. Regarding electrical machines, advances in terms of design methodology, optimization of existing topologies, development of new topologies, and improvements in cooling systems.

Specific technical requirements of electrical machines for powertrains are high torque/power density, high efficiency, wide speed range, and attractive costs [4]. Permanent Magnet Synchronous Machines (PMSM) meet several of these requirements and are, for this reason, widely used in vehicular powertrains. Specifically, Axial Flux Permanent Magnet (AFPM) machines have gained great interest because they have the advantages of PMSM with high levels of torque densities (Nm/m^3) and specific torque density (Nm/kg) [5]. Among AFPM machines, the YASA topology (Yokeless And Segmented Armature) stands out regarding high torque density and high efficiency [6].

One technical aspect that has not been explored in depth is the use of multiphase electrical machines for electric powertrains. The multiphase electrical machines and also their drive was initially developed for applications in high-power machines to operate with lower voltages and/or currents per phase, both in the inverter and machine. In addition, other advantages may be mentioned, such as reduction of torque ripple, reduction of power per phase, reduction in the harmonic content of the DC link current, and increase of power/torque density. Multiphase electrical machines can also be more fault-tolerant due to their inherent redundancy [7].

The YASA topology was originally envisioned as a medium-speed machine (1000 to 6000 rpm) for automotive applications with power below 200 kW [8]. However, there are examples of the use of this topology in applications such as electric aircraft, which demonstrates high performance with high current densities that will be required for takeoff [9], and hybrid electric vehicles such as the Regera hypercar [10].

The advantages of the YASA machine and multiphase machines were brought together in the work developed by [11]. In this work, a YASA machine was designed to improve the torque density of this topology through the increase of the number of phases in which the machine is fed. In particular, the machine was designed with the possibility

Eletrôn. Potên., Florianópolis, v. 28, n. 1, p. 17-27, jan./mar. 2023

17

of being connected with three, five, or fifteen symmetrical electrical phases. It was shown that torque density is improved and torque ripple is reduced with the increase in the number of phases. A following work has developed a multiphase inverter to test multi-star and multiphase electrical machines [12], and the machine designed by [11] was tested with several different electrical connections. It was shown in [12], e.g., that the multiphase machine does not lose synchronization even when one or two phases are open, which demonstrates the fault-tolerant characteristic of the multiphase machine. However, previous works have not developed and validated dynamic models, and have not elaborated Field-Oriented Control drives for a YASA machine that can operate with three or five phases. And the applicability of the YASA multiphase machine for electric powertrain has also not been found in the literature.

Based on the previous contextualization, the contributions of this paper are:

1. Dynamic modeling of the multiphase YASA machine that operates with three and five phases, performing only electrical reconnection;
2. Experimental determination of the dynamic model parameters from a prototype with three and five phases;
3. Validation and analysis of the drive and control of the YASA machine with three or five phases operating under conditions required by electric powertrains.

This work is organized as follows: In Section II the topology of the YASA machine and its constructive characteristics are described. Then, in Section III the machine dynamic models and control are addressed. In Section IV the conditions for the use of the machine in electric traction are presented. After, in Section V the experimental results are presented and discussed. Section V presents the main conclusions.

II. MULTIPHASE YASA MACHINE

The YASA machine, shown in Figure 1, is a synchronous rotating electrical machine with axial flux in the air gap, with two rotors and segmented armature [11]. The topology uses concentrated windings wound around each segment. The rotor is made of surface-mounted permanent magnets attached to a soft magnetic back-iron. Since the magnetic flux density vectors are mainly in the axial direction, due to the yokeless segmented armature, it is possible to use laminated electrical steel with oriented grains in this topology of electrical machine. This special feature of this topology allows obtaining even higher levels of torque per active volume, and higher power and efficiency [12]. The study carried out in this paper uses the prototype of the YASA machine designed in [11]. The main characteristics of this prototype are listed in Table I.

The prototype was designed to be fed with 3, 5, or 15 phases, according to the electrical configuration of its winding connections. To illustrate that it is possible to have symmetric back-emfs with the appropriate connection, Figure 2 shows the identification of the coils of a base machine used to build the resultant phasor diagrams. A base machine contains one complete symmetric system, and this machine was designed
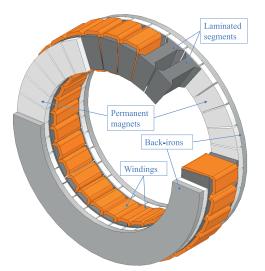

Fig. 1. Illustration of the electromagnetic components of the YASA machine.

TABLE I
Characteristics of the Prototype of the YASA Machine

Description	Value
Phase Number (m)	3 or 5
Number of Poles ($2p$)	32
Number of Slots (Q_a)	30
Turns per coil (Nc)	61
Outer rotor radius	80 mm
Inner rotor radius	56.57 mm
Inner stator radius	55.3 mm
Outer stator radius	81 mm
Stator length	30.89 mm
Back-iron thickness	4.23 mm
Magnet thickness (h_m)	4.5 mm
Air gap (g)	1 mm
Total axial length	50,35 mm
Active mass	3,64 kg
Armature segment material	Grain-oriented steel
Back-iron material	1020 carbon steel
Magnet material	NdFeB N40SH

to have two base machines with rotational symmetry in torque production. For this reason, only a half-section of the machine is shown in Figure 2. Considering that all coils are wound in the same direction, the back-emf phase voltages of the three-phase system $E_{3,1...3}$ are obtained connecting the coils according to Figure 3, whereas for the back-emf phase voltages of the five-phase system $E_{5,1...5}$, the coils are connected according to the phasor diagram of Figure 4.

It should be noted that the phasor diagrams shown in Figures 3 and 4 only consider the fundamental component of induced voltage. It should also be noted that the parameters of the lumped electrical model of the machine with three or five-phase connections are different. This particular aspect is addressed in the next section.
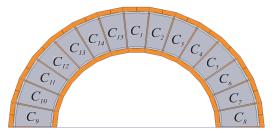
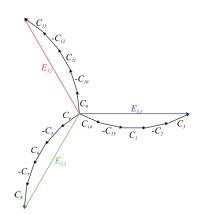Fig. 2. Identification of armature coils on the base machine [11].

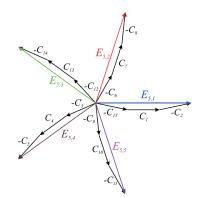Fig. 3. Phasor Diagram – 3 phase connection [12].

Fig. 4. Phasor Diagram – 5 phase connection [12].

III. DYNAMIC MODELS AND CONTROL

In this section the dynamic model of the machines with three or five phases is presented, the parameters of the dynamic model are determined, and the field-oriented control is discussed.

A. Dynamic Models

The electrodynamic model of lumped parameters with three and five phases can be realized in the synchronous reference frame (dq0). With this approach, the same model can represent the dynamic behavior of the machines with different electrical connections. The difference between the machine with these two electrical connections lies in the electromagnetic parameters. Therefore, the equations that can describe the dynamic model of the YASA machine with three or five phases are

$$v_d = R_s i_d + L_d \frac{di_d}{dt} - p\omega_m L_q i_q, \qquad (1)$$

$$v_q = R_s i_q + L_q \frac{di_q}{dt} + p\omega_m(L_d i_d + \psi_{pm}), \qquad (2)$$

and

$$T_e = J\frac{d\omega_m}{dt} + B\omega_m + T_L, \qquad (3)$$

where, v_d, v_q, are the voltages in the synchronous frame (d-q), ψ_{pm} the fundamental component of linkage magnetic flux produced by permanent magnets, L_q, L_d are the synchronous inductances, R_s the stator phase resistance, i_d, i_q the synchronous stator currents, ω_m the angular mechanical speed, p the number of pole pairs, T_e the electromagnetic torque, J the moment of inertia, B the friction coefficient, and T_L the load torque. The electromagnetic torque for the fundamental component of electric current for any of the electrical connections can be obtained from

$$T_e = \frac{m}{2}i_q p(i_d(L_d - L_q) + \psi_{pm}), \qquad (4)$$

where m is the number of phases.

The electromagnetic parameters ψ_{pm}, L_q, L_d, and R_s are different for the machine with three or five phases, meanwhile, the mechanical parameters J and B are the same.

B. Parameters of the Dynamic Model

The parameters of the dynamic model of the machine with three and five-phase connections were determined experimentally. It is important to highlight that the two groups of windings of the two base machines of the prototype are connected in series; therefore, the amplitude of the phase-induced voltage shown in the phasor diagrams of Figures 3 and 4 is multiplied by two. Obviously, the series connections between groups of windings also affect resistance, inductance, and linkage magnetic flux. Following, the experimental methods to obtain the parameters and the corresponding values are presented.

1) Resistance – R_s: The stator phase resistance R_s was obtained by applying 10 V DC between one phase and neutral terminals of the YASA machine. The measurement of the DC current allowed, through Ohm's Law, the determination of resistance. This procedure was repeated for all phases, in three-phase and five-phase configurations. The test was carried out at room temperature, between 15 ºC and 20 ºC and Figure 5 shows a schematic for three and five phases of how the test was performed.
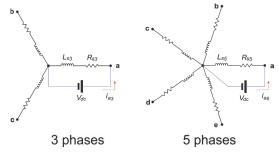

Fig. 5. Stator resistance measurement.

To collect the parameters, a DC Voltage Source and a DC

source oscilloscope, and Tektronix model MDO4054-3 with a current probe were used. The considered value corresponds to the average of the measurements between the phases of each configuration with a standard deviation (σ_R) of 26.6 mΩ.

2) Inductance – L_s: Since the YASA topology has surface-mounted magnets and no significant saturation is present in normal operation, the direct and quadrature-axis inductances are practically the same. In this way, it was considered that the stator inductance L_s is equal to the synchronous inductances, i.e., $L_s = L_d = L_q$. An additional relevant aspect is that the mutual inductance between non-adjacent phases is very low in this topology of electrical machines due to the segmented armature [11].

It must be mentioned that in the literature several methods are adopted for the measurement of synchronous inductances [13]. Considering the particularities of the YASA machine regarding inductances, a simple method was used, consisting of the application of DC step voltage. Thus, a step DC voltage of 10 V was applied with the positive terminal connected to a phase terminal and the negative terminal connected to two other adjacent phases, as shown in Figure 6 using the same equipment as in the previous section. Through the dynamic response of the current, the value of the RL circuit time constant [τ] is obtained, considering R_s determined according to the previous subsection.
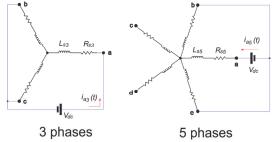

Fig. 6. Inductance measurement.

After the time constant is calculated, the value of the synchronous inductance for each measurement is obtained analytically with (5). The value of L_s was obtained by the average of the inductances obtained from the measurements applied to each phase terminal, with a standard deviation (σ_L) of 85.72 μH.

$$L_s = \frac{2}{3}\tau R_s \qquad (5)$$

For the five-phase machine, the applied step had the positive terminal connected to one phase and the negative terminal connected to the two adjacent phases. This method considers that mutual inductances in non-adjacent phases in the multiphase YASA machine are neglectable.

3) Linkage magnetic flux – ψ_{pm}: The linkage magnetic flux produced by the permanent magnets is determined based on the back-emf. Therefore the YASA machine is mechanically driven at constant speed by another machine and the open-circuit voltage of the YASA machine is acquired. With the voltage waveform, the FFT (Fast Fourier Transform) is performed in order to obtain the contribution of the

fundamental component of the phase back-emf E_{a1}. The ψ_{pm} is then determined according to (6).

$$\psi_{pm} = \frac{E_{a1}}{p\omega_m} \qquad (6)$$

Examples of the back-emf and its FFT of the three and five-phase YASA machine at 40 rad/s are shown in Figure 7.
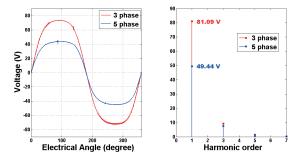

Fig. 7. Back-emf and corresponding FFT of the three and five-phase machines at 40 rad/s.

The electromagnetic parameters of the dynamic model of the YASA machine with three or five-phase connection is shown in Table II.

TABLE II
Electromagnetic Parameters of the YASA Prototype

Parameters	three-phase	five-phase
R_s	1.797 Ω	1.298 Ω
L_s	7.23 mH	4.41 mH
ψ_{pm}	126.98 mWb	77.20 mWb

4) Friction coefficient – B: The mechanical parameters were determined for the setup used for experimental validation described in Section V, i.e., a setup in which the shaft of the YASA machine is mechanically connected to a radial-flux PMSM machine (RFPMSM). The coefficient of friction *B* of each machine was obtained, according to (7), by measuring the mechanical torque at no load T_{mNL} and the mechanical speed. The friction coefficient of the YASA machine was measured driving the RFPMSM while the YASA machine terminals were disconnected, whereas the friction coefficient of the RFPMSM was measured driving the YASA machine while the terminals of the RFPMSM terminals were disconnected. The total friction coefficient of the experimental setup is the sum of both coefficients.

$$B = \frac{T_{mNL}}{\omega_m} \qquad (7)$$

5) Moment of Inertia – J: The moment of inertia was determined using deceleration curves, considering (8), where τ_n is the mechanical time constant obtained from the deceleration curve and *B* is the friction coefficient determined according to subsection III B.4.

$$J = B\tau_n \qquad (8)$$

The moment of inertia, as well as *B*, was also determined for the YASA machine and for the setup which contains the

RFPMSM. For the determination of the moment of inertia of the YASA machine, the mechanical shaft of the RFPMSM was decoupled. For both tests (with and without the RFPMSM) the YASA machine was driven to reach a steady state speed of 30 rad/s. After this condition was reached, the electrical supply was cut and the deceleration curve was measured. Results of the mechanical parameters are shown in Table III.

TABLE III
Mechanical Parameters

	Coefficient of friction	Moment of inertia
YASA	31.10 mNms	8.72 mkgm^2
Yasa+RFPMSM	41.81 mNms	15.50 mkgm^2

C. Field-Oriented Control

Among the fundamental principles of vector control is the mathematical conversion of an AC multiphase machine into an equivalent DC machine. In the rotor-referenced synchronous machine model, the currents i_q and i_d are constant at steady state operation with constant speed, which allows the use of classical control methods, such as PI controllers, which are suitable for following constant references. For the transformation of sinusoidal multiphase machines into dq0 references the Clarke-Park transformation can be used, which is presented in the generalized form for the fundamental component in (9). The variables g_d, g_q, and g_0 in (9) are quantities in the synchronous reference frame whereas the variables g_a, g_b, and g_m are the quantities of the multiphase sinusoidal system. Additionally, θ_r is the electrical rotor position and α is an electrical angle dependent on the number of phases, i.e., $\alpha = 2\pi/m$.

Since the dynamic models of the three-phase and five-phase machines can be described with the same equations, as discussed in Section III-A, the FOC diagram is also analogous. For example, for a speed reference ω_{ref} control with no flux-weakening operation, i.e., with $i_d = 0$, the FOC diagram implemented for the five-phase machine is the one shown in Figure 8.

The diagram of Figure 8 shows three controllers C_ω, C_{id} and C_{iq}, which are detailed in the following subsection.

D. Controllers Design

To design current controllers, the transfer function of the electrical model of the machine in coordinates dq0 must be considered, which are obtained by applying the Laplace Transform to equations (1), (2). The product between speed and currents in these equations results in a non-linear system. Although linearization techniques could be applied, the nonlinear elements of equations (1), (2) were disregarded, and decoupling axes components were considered disturbances. This approach can be adopted since the Proportional-Integral controller will make zero the steady-state error. Therefore the simplified transfer functions of the currents i_d and i_q are given by the respective equations

$$G_{vid}(s) = \frac{I_d(s)}{V_d(s)} = \frac{\frac{1}{L_s}}{s + \frac{R_s}{L_s}}, \qquad (10)$$

and

$$G_{viq}(s) = \frac{I_q(s)}{V_q(s)} = \frac{\frac{1}{L_s}}{s + \frac{R_s}{L_s}}. \qquad (11)$$

Through the transfer function of the mechanical model of the machine, the speed controller can be designed. The mechanical transfer function, based on (3) with $T_L = 0$, is given in

$$G_\omega(s) = \frac{\omega_m(s)}{T_e(s)} = \frac{\frac{1}{J}}{s + \frac{B}{J}}. \qquad (12)$$

In the present work, PI controllers were used for the current and speed loops. Its equations are:

$$
\begin{aligned}
C_{id} &= k_{pd} + \frac{k_{id}}{s} \\
C_{iq} &= k_{pq} + \frac{k_{iq}}{s} \\
C_\omega &= k_{p\omega} + \frac{k_{i\omega}}{s},
\end{aligned}
\qquad (13)
$$

where k_{pd}, k_{pq}, and $k_{p\omega}$ are proportional gains and k_{id}, k_{iq}, and $k_{i\omega}$ are integral gains of the i_d, i_q, and ω controllers, respectively.

The gains were designed aiming at canceling the plant pole at closed loop operation, so that the system has first-order behavior, as used in [14] and [15]. Therefore, the proportional and integral gains for current are described in 14 as:

$$
\begin{aligned}
k_{pd} &= k_{pq} = \omega_i L_s \\
k_{id} &= k_{iq} = \omega_i R_s,
\end{aligned}
\qquad (14)
$$

where ω_i is the bandwidth of the current controllers. For the determination of speed gains, a similar approach was adopted, i.e., the equations were determined by (15).

$$
\begin{aligned}
k_{p\omega} &= \omega_\omega J \\
k_{i\omega} &= \omega_\omega B,
\end{aligned}
\qquad (15)
$$

where ω_ω is the bandwidth for the speed controls. For the experimental and simulated tests, $\omega_i = 1570.7$ rad/s and $\omega_\omega = 12.56$ rad/s were used.

For the implementation in a digital system, the controllers obtained in the continuous time domain must be transformed into discrete signals, making the construction of the PI controllers' code simpler. The method used for discretization was the Tustin method, described in (16). The sampling frequency is $F_s = \frac{1}{T_s} = 40$ kHz. To obtain this sampling rate, the switching frequency is 20 kHz, according to the DSP configuration.

$$s = \frac{2}{T_s}\left(\frac{1 - z^{-1}}{1 + z^{-1}}\right) \qquad (16)$$

As shown in Figure 8, the current controllers set the voltages in the frame dq. In the discretized form the voltages v_d and v_q are determined respectively in the equations

Eletrôn. Potên., Florianópolis, v. 28, n. 1, p. 17-27, jan./mar. 2023

21

$$
\begin{bmatrix} g_d \\ g_q \\ g_{d3} \\ g_{q3} \\ \vdots \\ g_{dn} \\ g_{qn} \\ g_0 \end{bmatrix} = \sqrt{\frac{2}{m}} \begin{bmatrix} \sin\theta_r & \sin(\theta_r - \alpha) & \ldots & \sin(\theta_r + 2\alpha) & \sin(\theta_r + \alpha) \\ \cos\theta_r & \cos(\theta_r - \alpha) & \ldots & \cos(\theta_r + 2\alpha) & \cos(\theta_r + \alpha) \\ \sin 3\theta_r & \sin 3(\theta_r - \alpha) & \ldots & \sin 3(\theta_r + 2\alpha) & \sin 3(\theta_r + \alpha) \\ \cos 3\theta_r & \cos 3(\theta_r - \alpha) & \ldots & \cos 3(\theta_r + 2\alpha) & \cos 3(\theta_r + \alpha) \\ \vdots & \vdots & \vdots & \vdots & \vdots \\ \sin n\theta_r & \sin n(\theta_r - \alpha) & \ldots & \sin n(\theta_r + 2\alpha) & \sin n(\theta_r + \alpha) \\ \cos n\theta_r & \cos n(\theta_r - \alpha) & \ldots & \cos n(\theta_r + 2\alpha) & \cos n(\theta_r + \alpha) \\ \frac{1}{\sqrt{2}} & \frac{1}{\sqrt{2}} & \ldots & \frac{1}{\sqrt{2}} & \frac{1}{\sqrt{2}} \end{bmatrix} \begin{bmatrix} g_a \\ g_b \\ g_c \\ g_d \\ \vdots \\ g_{m-2} \\ g_{m-1} \\ g_m \end{bmatrix} \tag{9}
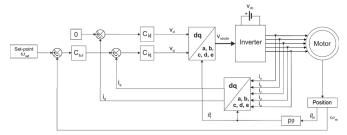$$

Fig. 8. FOC diagram of the five-phase YASA machine with speed reference.

$$
\begin{aligned}
v_{d(k)} =\ & (k_{pd} + \frac{k_{id}T_s}{2})e_{id(k)} + (\frac{k_{id}T_s}{2} - k_{pd})e_{id(k-1)} \\
& + v_{d(k-1)},
\end{aligned} \tag{17}
$$

and

$$
\begin{aligned}
v_{q(k)} =\ & (k_{pq} + \frac{k_{iq}T_s}{2})e_{iq(k)} + (\frac{k_{iq}T_s}{2} - k_{pq})e_{iq(k-1)} \\
& + v_{q(k-1)},
\end{aligned} \tag{18}
$$

where (k) represents the current value and $(k-1)$ means the previous value.

The reference for the current control i_q is provided by the speed loop, according to the equation

$$
\begin{aligned}
i_{qref(k)} =\ & (k_{p\omega} + \frac{k_{i\omega}T_s}{2})e_{\omega(k)} + (\frac{k_{i\omega}T_s}{2} - k_{p\omega})e_{\omega(k-1)} \\
& + i_{qref(k-1)}.
\end{aligned} \tag{19}
$$

IV. APPLICATION IN ELECTRIC TRACTION

Driving cycles were primarily developed to check emissions and fuel consumption. In electric vehicles, driving cycles are used to verify performance in terms of power demands and energy consumption. They are intended to match realistic driving patterns in different conditions where the vehicle speed is constantly changing and the performance of all other parts of the system is also highly variable.

The ECE-15 cycle is representative of urban driving conditions in a typical European city like Paris or Rome. It consists of several driving modes of constant acceleration, deceleration, and speed. The ECE-15 is characterized as a legislative cycle, that is imposed by governments as a procedure that all new types of vehicles have to follow for their emission certification. Four segments of the ECE-15 and one of the Extra Urban Driving Cycle (EUDC) form the New

European Driving Cycle (NEDC), implemented in the year 2000. The NEDC is used by European Union countries for the certification of passenger cars and light trucks [16].

The ECE-15 cycle is used to test the performance of small vehicles with speeds up to 50 km/h [17]. The adopted values are compatible with the speed and torque parameters that can be produced by the YASA machine prototype used in this work.

The torque that must be developed by the electrical machine during the driving cycle can be estimated using classical equations presented in the literature for vehicle dynamics [18]. For example, equation 20 allows determining torque produced by the motor T_m for a given set of vehicle parameters, a given acceleration, and with a flat surface.

$$
\frac{G}{r}T_m = \mu_{rr}mg + 0.625 A C_d v^2 + (m + \frac{JG^2}{n_g r^2})\frac{dv}{dt}, \tag{20}
$$

where G is the transmission ratio, r the radius of the wheel, m the mass of the vehicle, g the acceleration of gravity, A the frontal area of the vehicle, μ_{rr} the rolling friction coefficient, C_d the aerodynamic coefficient, v the linear speed of the vehicle, J the moment of inertia of the rotating parts, and n_g the efficiency of the system.

Considering the dynamic model and the vector control of the machine with 3 and 5 phases presented in Section III, the ECE 15 driving cycle curve as the speed reference and (20), it was possible to evaluate the dynamic response of the YASA machine applied to electric traction.

Results of speed and torque of the YASA machines with three and five-phase operation are shown in Figure 9.a and Figure 9.b, respectively. For this analysis parameters of a small vehicle, such as a scooter, were considered. Additionally, it was considered that it is a direct drive system. The adopted parameters were: $G = 1$, $r = 0.21$ m, $m = 185$ kg, $g = 9.81$ m/s^2, $A = 0.6$ m^2, $C_d = 0.75$, $\mu_{rr} = 0.007$, $J = 0.4278$ kgm^2 and $n_g = 0.95$.

Through the simulation performed with the computational tool Matlab/Simulink, it is verified that the YASA motor prototype is able to follow the speed reference and can provide the required torque with similar behavior for the three-phase and five-phase configurations.

V. EXPERIMENTAL RESULTS AND DISCUSSION

The experimental setup is composed of the power inverter and the YASA machine installed on a test bench with the RFPMSM.

The inverter used was developed in [19]. It contains

22

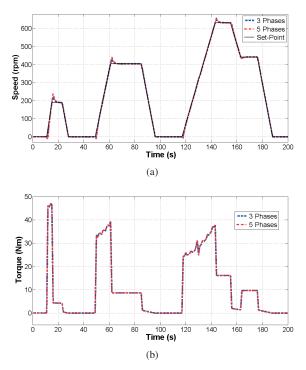Eletrôn. Potên., Florianópolis, v. 28, n. 1, p. 17-27, jan./mar. 2023

Fig. 9. Computer simulation of (a) speed and (b) torque of the YASA machine with three and five phases under ECE-15 drive cycle.

a Texas Instruments DSP (model TMS320F28379D), which has two 32-bit cores, floating point operation, and a base clock of 200 MHz, which is responsible for reading the input signals, executing the control algorithm and modulating the output signals through the gate drives. The inverter was initially developed to drive independently two three-phase electrical machines, but it can be used to drive a five-phase machine since it contains six IGBT inverter legs that can be independently controlled. In this way, the inverter can drive and control the YASA machine configured with three or five-phase connection. A photograph of the inverter is shown in Figure 10.
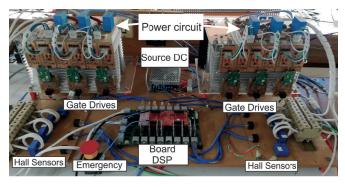

Fig. 10. Power inverter used for driving the prototype.

To complete the experimental setup, the shaft of the YASA prototype is fixed to a torquemeter and then to the shaft of the RFPMSM as shown in Figure 11. An encoder is also attached to the shaft of the YASA machine, which is used for speed measurement and for determining the rotor's position for the implementation of FOC.

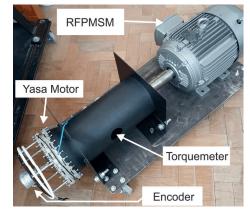Figure 12 displays a schematic block diagram of the entire

Fig. 11. YASA machine coupled RFPMSM and torquemeter.

implemented system that performs the YASA motor vector control for three or five phases.
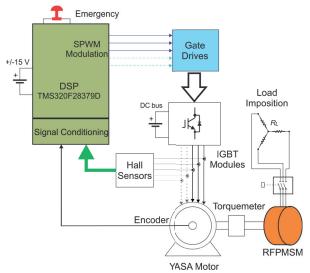

Fig. 12. Schematic diagram of the implemented system.

Aiming the validations of the dynamic model and of the FOC developed for the three-phase and five-phase YASA machine, tests were performed for both connections operating with no mechanical load and with the mechanical load. The mechanical load was imposed by using the RFPMSM as a generator feeding balanced three-phase resistive loads. It should be noted that due to this method, the torque value changes with the variation of the angular speed once the resistive load is kept constant. Finally, to demonstrate that the multiphase YASA machine can operate under conditions required for electric traction, a speed reference equivalent to the ECE-15 driving cycles was imposed.

The limit values of the inverter and the test bench are described in the Table IV.

TABLE IV
Experimental Bench Limits

Description	Value
DC Link Voltage	500 V
Current per Phase (IGBT)	200 A
Switching Frequency	50 kHz
Mechanical Angular Velocity	50 rad/s
Load Torque	10 Nm

A. Three-Phase Test

First, the three-phase YASA machine was driven under no-load conditions imposing as reference steps of 10 rad/s starting from 10 rad/s up to 40 rad/s. The experimental results of speed, quadrature current, and quadrature voltage are compared to the results obtained from the dynamic model as shown in Figure 13. It can be observed that speed reference is followed and the machine electrical quantities i_q and v_q are in good agreement with the mathematical model, which validates both the model and the developed FOC.
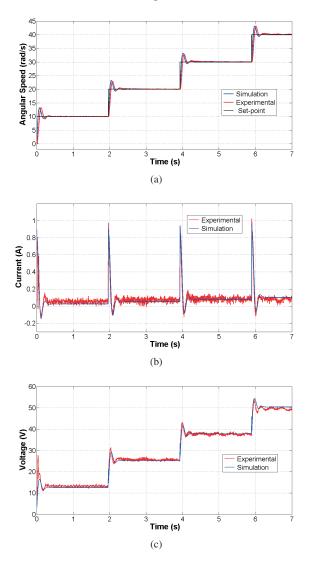

(a)

(b)

(c)

Fig. 13. No-load speed steps of the three-phase YASA machine (a) Mechanical Angular Speed (b) Current i_q (c) Voltage v_q.

After, a mechanical load was imposed on the YASA three-phase machine by connecting balanced electrical resistive loads to the three-phase terminals of the RFPMSM. In this test two speed reference steps of 10 rad/s for applied. The speed, quadrature, and direct-axis currents were measured and compared to the model as shown in Figure 14.

Again, the speed reference shown in Figure 14.a is followed and the electrical quantities show good agreement with the mathematical model. On the other hand, the current i_q shown in Figure 14.b, presents peak amplitudes during transitions in the experimental curve higher than those obtained in the
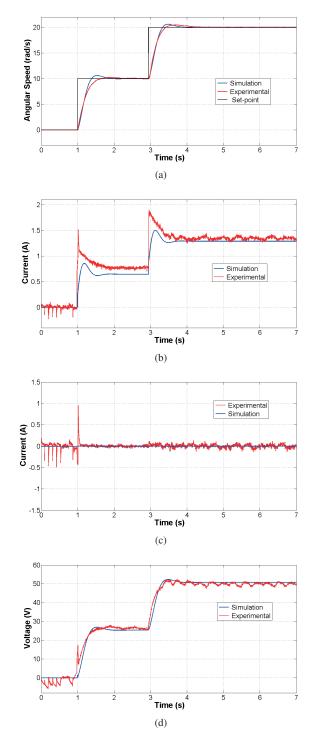

(a)

(b)

(c)

(d)

Fig. 14. Speed steps of the three-phase YASA machine with a load of 2.08 Nm at 20 rad/s (a) Mechanical Angular Speed (b) Current i_q (c) Current i_d (d) Voltage v_q.

simulated values. This discrepancy is possibly associated with some difference between the real value and the value considered in the analytical model of the system's moment of inertia, because during transitions this element is the one with the greatest influence on the load torque. In steady state operation, there is a difference in the level of i_q, which indicates that the experimental load torque is higher than the one considered in our simplified model of the load imposed by the RFPMSM. One possible reason to explain the discrepancy

is the fact that the rotational losses of the RFPMSM were not considered to model the load. Besides the i_q current, the quantities are in good agreement in the steady state operation. Moreover, all no-load test curves are very close, allowing to consider that the dynamic model of the three-phase YASA machine is validated with the parameters obtained in Section III.

B. Five-Phase Test

The YASA machine with a five-phase connection was submitted to similar tests as the three-phase configuration, i.e., driven under no-load conditions imposing as reference steps of 10 rad/s starting from 10 rad/s up to 40 rad/s and under load with 10 rad/s and 20 rad/s.

Experimental and model results for no-load operation in terms of speed, quadrature current, and quadrature voltage are shown in Figure 15. Comparatively, the experimental and model results show good agreement, which also validates the dynamic model and the FOC developed for the five-phase machine.
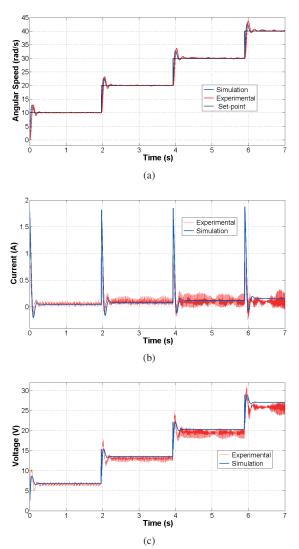

(a)

(b)

(c)

Fig. 15. No-load speed steps of the five-phase YASA machine (a) Mechanical Angular Speed (b) Current i_q (c) Voltage v_q.

If the no-load results for the three-phase machine, shown

in Figure 13 are compared to the no-load results for the five-phase machine, shown in Figure 15, it is possible to conclude that both dynamic models are well-represented and that the amplitude of quadrature voltage applied in the five-phase machine is lower for the same speed. This last aspect is expected since the fundamental component of phase voltage is lower in the five-phase machine, as demonstrated in Figure 7.
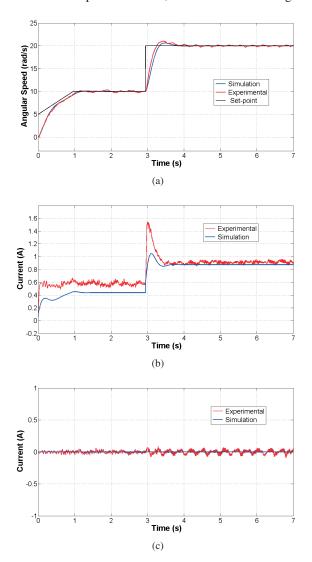

(a)

(b)

(c)

Fig. 16. Speed steps of the five-phase YASA machine with load of 2.08 Nm at 20 rad/s (a) Mechanical Angular Speed (b) Current i_q (c) Current i_d.

Experimental and model results under mechanical load in terms of speed, quadrature, and direct-axis currents are shown in Figure 16. The velocity curves follow the imposed reference and show good compatibility between the simulated and experimental values. However, slight oscillations in the experimental speed are observed even when the steady state is reached. It is believed that these oscillations are due to the existence of the third harmonic component of the current that circulates in the five-phase configuration that produces torque oscillations, since in the determination of the model, only the fundamental component was considered. As with the three-phase test, the current curves i_q shown in Figure 16.b are different in the peak value of the quadrature current during

Eletrôn. Potên., Florianópolis, v. 28, n. 1, p. 17-27, jan./mar. 2023

25

the transition, which we believe to be related to the value of the moment of inertia and experimental rotational losses, as detailed in the previous subsection.

C. Driving Cycle Test

To show the applicability of the multiphase YASA machine to electric traction, the five-phase configuration of the prototype was driven following a speed reference with a format equivalent to the ECE-15 driving cycle. However, due to limitations in the storage time in the control unit, the ECE-15 cycle, which has a runtime of 200 seconds, was reduced to 16 seconds. The format of the driving cycle was proportionally adjusted to maintain the original format. Also, a maximum speed of 382 rpm at the machine was applied due to the limitations of the mechanical setup. For a direct-drive system of a scooter-type vehicle, the ECE-15 driving cycle would require a maximum rotation of 631.6 rpm.

The main objective of the test carrying out was to verify the experimental behavior of the machine during a typical driving cycle following the imposition of the speed reference curves. An experimental test for the ECE-15 driving cycle with adjusted runtime was carried out without mechanical load. The transitions and operation with load caused high levels of vibration in the setup. However, a static test carried out with this prototype and detailed in [11] showed that the machine produces torque in the range of 40 Nm, as required according to Figure 9.b. Figure 17 displays the experimental and simulated results for speed obtained for the test as described.
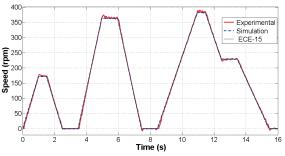

Fig. 17. Speed of the multiphase YASA under ECE-15 equivalent driving cycle.

This test demonstrated that the YASA multiphase machine with the developed FOC can provide the dynamic response necessary in electric traction applications.

VI. CONCLUSIONS

This work presented the YASA-type electrical machine conceived to operate with a symmetric and balanced three-phase or five-phase configuration. A dynamic model of the machine for both configurations was addressed and the parameters of this model were experimentally determined. The FOC was designed for both configurations. Additionally, the method of determining the appropriate electric machine for a particular electric vehicle was presented, acting under a specific driving cycle. Finally, experimental and mathematical model results were compared.

The experimental results validated the dynamic models of the machines, with the parameters obtained experimentally.

Therefore, it was demonstrated that the same electromagnetic model in the synchronous reference frame can represent the dynamic behavior of a three-phase and five-phase YASA machine.

Simulations of the YASA machine with three-phase and five-phase configurations driving an electric vehicle such as a scooter under a driving cycle (ECE-15) were performed. Simulation results show that both configurations can be used and have similar behavior in terms of dynamic response for the cases analyzed. Experimental results with similar conditions demonstrated that the multiphase YASA machine follows the speed reference of a simplified ECE-15 driving cycle with the developed FOC.

REFERENCES

[1] I. López, A. Matallana, J. Andreu, I. Kortabarria, "Next generation electric drives for HEV/EV propulsion systems: Technology, trends and challenges", *Renewable and Sustainable Energy Reviews*, vol. 114, p. 109336, Jul./Ago. 2019.

[2] IEA, "Global EV Outlook 2020", *International Energy Agency*, p. 276, Abr. 2020.

[3] F. Savi, D. Barater, M. D. Nardo, M. Degano, C. Gerada, P. Wheeler, G. Buticchi, "High-Speed Electric Drives: A Step Towards System Design", *IEEE Open Journal of the Industrial Electronics Society*, vol. 8, no. 1, pp. 10–21, Jan. 2020.

[4] R. Benlamine, F. Dubas, C. Espanet, S. Randi, D. Lhotellier, "Design of an Axial-Flux Interior Permanent-Magnet Synchronous Motor for Automotive Application: Performance Comparison with Electric Motors used in EVs and HEVs", *IEEE Transactions on Instrumentation and Measurement*, Abr. 2014.

[5] R. Krishnan, *Permanent Magnet Synchronous and Brushless DC Motor Drives*, CRC Press, Boca Raton., 2010.

[6] T. Woolmer, M. McCulloch, "Analysis of the Yokeless And Segmented Armature Machine", *IEEE International Electric Machines and Drives Conference*, pp. 1574–1579, Maio 2007.

[7] R. S. Miranda, C. B. Jacobina, A. M. N. Lima, M. B. R. Corrêa, L. A. S. Ribeiro, "Operação de um Sistema De Acionamento com Motor de Seis Fases Tolerante a Faltas", *SOBRAEP – Revista Eletrônica de Potência*, vol. 10, no. 1, pp. 15–22, Jun. 2005.

[8] S. T. Vun, M. D. McCulloch, "Optimal Design Method for Large-Scale YASA Machines", *IEEE Transaction on Energy Conversion*, vol. 30, no. 3, pp. 900–907, Set. 2015.

[9] D. Talebi, M. C. Gardner, S. V. Sankarraman, A. Daniar, H. A. Toliyat, "Electromagnetic Design Characterization of a Dual Rotor Axial Flux Motor for Electric Aircraft", *IEEE International Electric Machines and Drives Conference*, 2021.

[10] I. Aghabali, J. Bauman, P. J. Kollmeyer, Y. Wang, B. Bilgin, A. Emadi, "800-V Electric Vehicle Powertrains: Review and Analysis of Benefits, Challenges, and Future Trends", *IEEE Transactions*

26

Eletrôn. Potên., Florianópolis, v. 28, n. 1, p. 17-27, jan./mar. 2023

on *Transportation Electrification*, vol. 7, no. 3, pp. 927–948, Set. 2021.

[11] E. C. Goltz, *Estudo da Máquina Elétrica de Fluxo Axial com Duplo Rotor e Armadura Segmentada*, Ph.D. thesis, Universidade Federal do Rio Grande do Sul, Porto Alegre, 2016.

[12] R. Parizotto, E. C. Goltz, E. Reis, P.R.Eckert, "Design and Development of a Multiphase Inverter for Automotive Applications", *SOBRAEP – Revista Eletrônica de Potência*, vol. 27, no. 2, pp. "139–148", Jun. 2022.

[13] V. Rallabandi, N. Taran, D. Ionel, P. Zhou, "Inductance Testing for IPM Synchronous Machines According to the New IEEE Std 1812 and Typical Laboratory Practices", *IEEE Transactions on Industry Applications*, vol. 55, no. 3, pp. 2649–2659, Maio–Jun. 2019.

[14] A. M. Diab, F. Guo, G. Buticchi, S. S. Yeoh, M. Galea, "Fast and Simple Tuning Rules of Synchronous Reference Frame Proportional-Integral Current Controller", *IEEE Acess*, vol. 9, pp. 22156–22170, Jan. 2021.

[15] L. C. Borin, C. R. Osório, G. Koch, T. S. Gabbi, R. C. Oliveira, V. F. Montagner, "Robust Control Design Procedure Based on Particle Swarm Optimization and Kharitonov's Theorem With an Application for PMSMs", *SOBRAEP – Revista Eletrônica de Potência*, vol. 25, no. 2, pp. 219–229, Jun. 2020.

[16] E.Tzikaris, K. Pitsas, F. Zannikos, S. Stournas, "Vehicle Emissions and Driving Cycles: Comparison of the Athens Driving Cycle (ADC) With ECE-15 and European Driving Cycle (EDC)", *Global NEST Journal*, vol. 8, no. 3, pp. 282–290, Nov. 2006.

[17] I. P. Wiltuschnig, *Projeto e Dimensionamento de um Sistema de Tração para Veículos Elétricos*, Master's thesis, Universidade Federal do Rio Grande do Sul, Porto Alegre, 2016.

[18] J. Larminie, J. Lowry, *Electric Vehicle Technology Explained*, John Wiley, London, UK, 2012.

[19] T. Lazzari, *Desenvolvimento de Sistemas de Controle para Motores de Imãs Permanentes para Tração de Veículos Elétricos*, Master's thesis, Universidade Federal de Santa Maria, Santa Maria, 2020.

BIOGRAPHIES

Ederson dos Reis was born in Caxias do Sul, Brazil, RS in 1975. He received a degree in Electrical Engineering from the University of Caxias do Sul (UCS) in 2015, and the M.Sc. degree in Electrical Engineering from the Federal University of Rio Grande do Sul (UFRGS), Porto Alegre, RS, Brazil, in 2022. He is currently a managing partner of the company Style Equipamentos Eletrônicos. He has experience in the field of electrical engineering, with an emphasis on industrial electronics and electronic device development. His research interests include control and drive of electrical motors and the design and modeling of power inverters.

Rodrigo Parizotto was born in São Marcos, RS, Brazil, in 1987. He received the B.Eng. degree in Electrical Engineering from the University of Caxias do Sul (UCS) in 2015, and the M.Sc. degree in Electrical Engineering from the Federal University of Rio Grande do Sul (UFRGS), Porto Alegre, RS, Brazil, in 2021. He is currently Project Manager in the company Inbrasel, working with the research and development of industrial machines. His research interests include the design and modeling of power inverters applied to electric mobility.

Lucas Rossato Rocha was born in Santa Maria, RS, Brazil in 1995. He received the B.S. and Ms. in Electrical Engineering from Federal University of Santa Maria (UFSM) in 2019 and 2021. He is currently a Ph.D student at the Federal University of Santa Maria (UFSM). His main research interests include control and drive of electrical motors, control of non-sinusoidal PMSM, design and analysis of observers and study of techniques to reduce torque ripple in non-sinusoidal PMSM.

Evandro Claiton Goltz received the B.Eng. degree in electrical engineering from the Federal University of Santa Maria (UFSM), Santa Maria, RS, M.Eng. and Ph.D. degrees in electrical engineering from the Federal University of Rio Grande do Sul (UFRGS), Porto Alegre, RS, Brazil, in 2009, 2012 and 2021, respectively. Currently he is working with NUPEDEE/UFSM with the Laboratory of Electrical Machines. His research interests include design and modeling of electromagnetic devices and electric drives. Dr. Goltz is a member of the Brazilian Society of Electromagnetism.

Rodrigo Padilha Vieira was born in Cruz Alta, Brazil. He received the B.S. degree in Electrical Engineering from the Universidade Regional do Noroeste do Estado do Rio Grande do Sul, Ijuí Brazil, in 2007, and the M.Sc. and Dr. Eng. degrees in Electrical Engineering from the Federal University of Santa Maria (UFSM), Santa Maria, Brazil, in 2008 and 2012, respectively. From 2010 to 2014, he was with the Federal University of Pampa, Alegrete, Brazil. Since 2014, he has been with the UFSM, where he is currently a Professor of Electrical Machines. His research interests include electrical machine drives, sensorless drives, digital control techniques of static converters.

Paulo Roberto Eckert received the B.Eng., M.Sc. and Ph.D. degrees in electrical engineering from the Federal University of Rio Grande do Sul (UFRGS), Porto Alegre, RS, Brazil, in 2007, 2012, and 2016, respectively. He is currently an Associate Professor with the Department of Electrical Enginnering and a Researcher with the Laboratory of Electrical Machines, Drives and Energy, UFRGS. His research interests include design and modeling of electromagnetic devices and electric drives.

Eletrôn. Potên., Florianópolis, v. 28, n. 1, p. 17-27, jan./mar. 2023

27